PHILOSOPHICAL TRANSACTIONS OF THE ROYAL SOCIETY A MATHEMATICAL, PHYSICAL & ENGINEERING SCIENCES

A first-principles characterization of water adsorption on forsterite grains

Abu Md Asaduzzaman, Slimane Laref, P. A. Deymier, Keith Runge, H.-P. Cheng, Krishna Muralidharan and M. J. Drake

Phil. Trans. R. Soc. A 2013 **371**, 20110582, published 3 June 2013

PHILOSOPHICAL TRANSACTIONS OF THE ROYAL SOCIETY A

rsta.royalsocietypublishing.org

Research

Cite this article: Asaduzzaman AM, Laref S, Deymier PA, Runge K, Cheng H-P, Muralidharan K, Drake MJ. 2013 A first-principles characterization of water adsorption on forsterite grains. Phil Trans R Soc A 371: 20110582.
http://dx.doi.org/10.1098/rsta.2011.0582

One contribution of 11 to a Theme Issue 'Surface science in the interstellar medium'.

Subject Areas:
geochemistry, interstellar medium, computational chemistry, astrochemistry

Keywords:
endogenous water, adsorption, mechanisms, forsterite, density functional theory, dissociation

Author for correspondence:
Krishna Muralidharan
e-mail: krishna@email.arizona.edu

†In memory of Prof. Michael J. Drake

A first-principles characterization of water adsorption on forsterite grains

Abu Md Asaduzzaman[1,2], Slimane Laref[2], P. A. Deymier[2], Keith Runge[2,3], H.-P. Cheng[3], Krishna Muralidharan[1] and M. J. Drake[1,†]

[1]Lunar and Planetary Laboratory, and [2]Material Science and Engineering, University of Arizona, Tucson, AZ 85721, USA
[3]Quantum Theory Project, University of Florida, Gainesville, FL 32611, USA

Numerical simulations examining chemical interactions of water molecules with forsterite grains have demonstrated the efficacy of nebular gas adsorption as a viable mechanism for water delivery to the terrestrial planets. Nevertheless, a comprehensive picture detailing the water-adsorption mechanisms on forsterite is not yet available. Towards this end, using accurate first-principles density functional theory, we examine the adsorption mechanisms of water on the (001), (100), (010) and (110) surfaces of forsterite. While dissociative adsorption is found to be the most energetically favourable process, two stable associative adsorption configurations are also identified. In dual-site adsorption, the water molecule interacts strongly with surface magnesium and oxygen atoms, whereas single-site adsorption occurs only through the interaction with a surface Mg atom. This results in dual-site adsorption being more stable than single-site adsorption.

1. Introduction

There has been an ongoing debate on the origin of water on the Earth and other inner-Solar System planets [1–3]. So far, there is no consensus regarding the water-delivery mechanism(s). The recent discovery of the comet 103P/Hartley 2 containing water that is similar in isotopic composition to that in the Earth's oceans indicates that comets may well have played an important

role in delivering water to the Earth exogenously [4]. Morbidelli *et al*. [3] have shown that a significant fraction of the Earth's mass could be accreted late as a result of collisions with asteroids originating in the Main Belt. This could have resulted in water delivery, though the Os isotope ratio in the Earth's mantle imposes a constraint on asteroids as being the dominant source of the Earth's water. In contrast to the above exogenous scenarios, Drake [5] hypothesized that some of the Earth's water could be endogenous, with the delivery occurring via direct adsorption of water onto grains in the accretion disc, given that water and solid particulates coexisted in the accretion disc prior to planet formation. Specifically, it has been established that grains of olivine, pyroxenes and other refractory minerals [6] in the presence of water vapour and hydrogen made up the dust cloud around the young solar objects. The estimation of lifetime of these gases in the accretion disc varies over a wide range from 0.1 to 10 Myr [7]. Even the lowest lifetime estimates should allow sufficient time for water adsorption, and if water is adsorbed strongly onto dust grains during the early stages of accretion, then permanent water incorporation within the rocky terrestrial planets is very likely.

Towards this end, several computational investigations examining the adsorption process on forsterite (i.e. Mg-end member of olivine) surfaces have been carried out [8–12] and have provided the energetics of both associative [10] as well as dissociative adsorption [8,9] of water. The obtained energetics for certain associative and dissociative adsorption geometries exceeded 1.5 eV (approx. 150 kJ mol^{-1}), and, based on Muralidharan *et al*. [12], it can be inferred that the adsorbed water molecules would remain stable on the grains even at conditions corresponding to early stages of accretion (i.e. high temperature and low partial pressure). Further, Elkins-Tanton [13] has demonstrated that the formation of surface oceans on the Earth should be possible, provided that the accreting building blocks contain water.

The above investigations [8–12] represent important milestones in establishing the possibility of adsorption as a possible water-delivery source to the Earth; still, it needs to be pointed out that these results were obtained using differing levels of theory and computational complexity. For example, previous studies [8–10] use classical simulations that invoke suitably parametrized interatomic potentials to model their systems, whereas Goumans *et al.* [11] rely on a combination of density functional theory (DFT) in conjunction with empirical molecular mechanics methods to study the energetics of adsorption. Further, it should be noted that the above studies used very small periodic supercells in their simulations, possibly constraining the adsorption geometries and thereby the adsorption energetics. Thus, in this work, by solely using rigorous DFT calculations and examining larger supercells, we propose to verify and extend current understanding of water adsorption on different forsterite surfaces. Both associative and dissociative water adsorption are examined; particular attention is paid to the interplay between the relative orientation of the water molecule and the surface atomic structure in addition to studying multi-molecular adsorption in greater detail than has been carried out previously, enabling a rigorous understanding of the nuances of the water-adsorption process on different forsterite surfaces.

2. Computational procedure

To enable the characterization of the adsorption process, we carry out computational studies based on the plane-wave DFT method using larger supercells than were used in previous investigations. The modes of adsorption (associative versus dissociative), various adsorption geometries as mediated by the different surface atoms, and adsorption energy on the (100), (001), (010) and (110) surfaces of forsterite are presented, analysed and discussed. Unless otherwise noted, our calculations have been performed using the plane-wave code Vienna Ab initio Simulation Package (VASP), v. 4.6 [14,15], within the framework of Kohn–Sham DFT and the generalized gradient approximation functional Perdew–Burke–Ernzerhof [16]. We have used the projected augmented wave method [15,17], as provided within the VASP package [18], to treat the core-electron states of the different atoms. For magnesium, we treat the semi-core 2*p* electrons explicitly. A cut-off energy of 400 eV has been chosen for the plane-wave basis.

In order to simulate the different surfaces, a $(2 \times 2 \times 1)$ periodic supercell consisting of 112 atoms was used, with a vacuum region of 15 Å separating the periodic images of the slab, each approximately 12 Å thick. An adequately sized vacuum region prevents spurious interactions between periodic supercells. In addition, some test calculations were also performed using an 18 Å vacuum region, and no notable dependence on the vacuum region size was noticed. For each system, the bottom-layer atoms were fixed at positions corresponding to the bulk configuration, whereas all other atoms were allowed to relax. Because of the large size of the supercell, a $2 \times 2 \times 1$ Monkhorst–Pack [19] k-points grid was used. The characteristics of all four surfaces are different and, hence, we have presented the results on all four surfaces. It should be noted that the DFT simulation parameters were chosen to ensure that the relevant parameters such as lattice constants matched those of experiments within 1 per cent [20]. The surfaces were then generated from the optimized bulk structure ($a = 10.19$ Å, $b = 4.77$ Å, $c = 6.03$ Å). Specifically, all surfaces reported in this study were generated as a non-polar surface, i.e. created by only allowing the cleaving Mg−O bonds while keeping the SiO_4 unit intact. The cleaved surfaces were then relaxed, with the relaxation energy of each surface given by equation (2.1),

$$E_r = \frac{E_{sr} - E_{sur}}{A}, \tag{2.1}$$

where E_{sr} and E_{sur} represent the energy of the relaxed and the unrelaxed surfaces, respectively, whereas A is the corresponding surface area.

The energetics of associative and dissociative adsorption of water on the relaxed forsterite surfaces were obtained from equation (2.2),

$$\Delta E = E_{hyd} - E_{sr} - E_W, \tag{2.2}$$

where ΔE, E_{hyd} and E_W represent the adsorption energy, hydration energy owing to adsorption of a single water molecule and the cohesive energy of a water molecule, respectively. For the sake of simplicity, we report only the magnitude of ΔE; larger ΔE implies stronger adsorption.

Dissociation was studied by allowing the constituents of the water molecule, namely the hydroxyl (OH) and the hydrogen atom, to adsorb on two different adsorption sites, in contrast to associative adsorption, in which the water molecule was allowed to adsorb onto 'active' surface atomic sites, while ensuring that the integrity of the water molecule was retained. The active sites for adsorption were identified based on the under-coordinated magnesium and oxygen atoms (when compared with bulk coordination) present on or close to the surface.

3. Results and discussion

The surface relaxation energy of the geometry-optimized (010), (100), (001) and (110) surfaces is reported in table 1. The surface relaxation energy of (100) was the lowest, whereas that of (010) was the highest among the four surfaces. It may be of note that our calculated trend for surface relaxation energies is in agreement with the previously reported [21,22] surface energies. The optimized structures of four surfaces are shown in figure 1.

Using the geometry-optimized structures, we next examined adsorption of a single water molecule on the different surfaces. A summary of the structural features and energetics corresponding to water adsorption is given in tables 2 and 3, respectively, whereas a more detailed case-by-case study for each surface is discussed below. Note that the energies given in table 3 correspond to strong exothermic adsorption, and, based on the work of Muralidharan *et al.* [12], structural stability of the hydrated surfaces can be expected even at elevated temperatures corresponding to the accretion disc.

(a) Water adsorption on the (100) surface

The (100) surface was characterized by two active magnesium (Mg) adsorption sites and one oxygen (O_s) site per unit cell (i.e. eight Mg and four O_s for the 2×2 supercell used in this

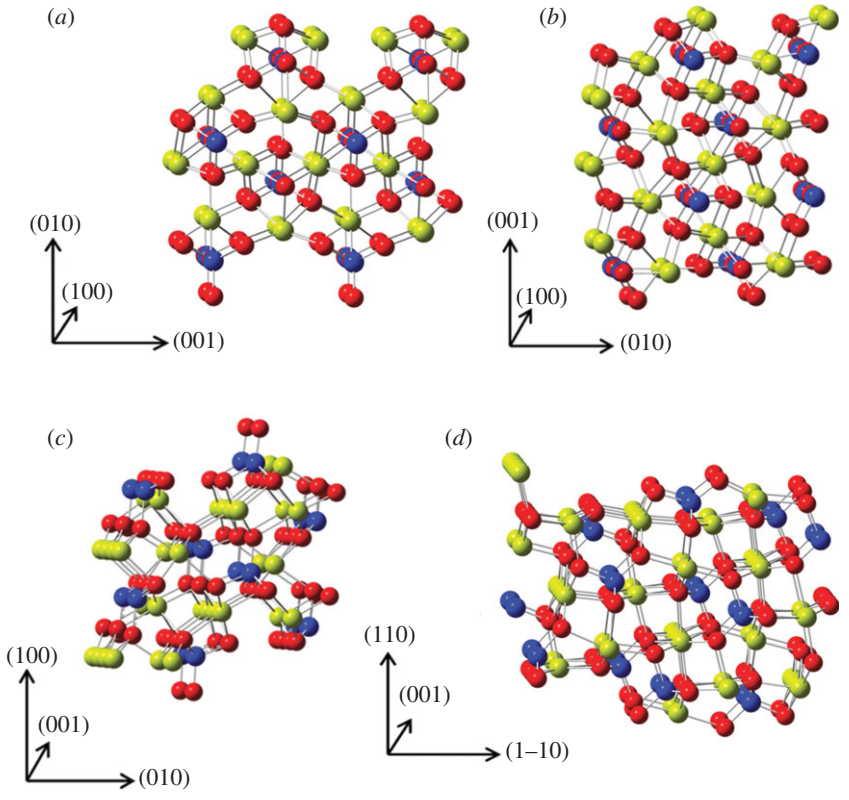

Figure 1. The optimized forsterite surfaces. (*a*), (*b*), (*c*) and (*d*) correspond to (100), (001), (010) and (110) surfaces, respectively. The yellow, blue and red spheres represent Mg, Si and O atoms, respectively.

Table 1. Surface relaxation energies (E_r) in eV/Å^2 of (010), (100), (001) and (110).

	surfaces			
	(100)	(001)	(010)	(110)
E_r	0.02	0.03	0.06	0.03

Table 2. Mg–O_w, O_s–O_w and O_s–H_w distances (Å) in the adsorption of water on the (100), (001), (010) and (110) surfaces.

adsorption mode	adsorption site/configuration	(100)		(001)		(010)			(110)	
		Mg—O	O—H	Mg—O	O—H	Mg—O	O—O	O—H	Mg—O	O—H
associative	Mg/single site	2.09		2.02		2.09			2.10	
	Mg/dual site	2.07	1.64	1.96	1.38					
dissociative	Mg	1.92	0.97	1.94	0.98	1.92		1.04/1.53[a]	2.02	0.97
	O						1.49	0.97		

[a]Distance between H_w and next neighbour O_s.

work). Two primary configurations, both mediated by surface Mg atoms, were identified for associative water adsorption—the single-site and dual-site adsorption geometries as shown in figure 2. Specifically, in single-site adsorption, the oxygen atom (O_w) of the water molecule bonds to the surface Mg, with the hydrogen atoms (H_w) pointing away from the surface. Alternatively, in the dual-site adsorption, the O_w interacts with Mg, whereas one H_w forms a secondary hydrogen

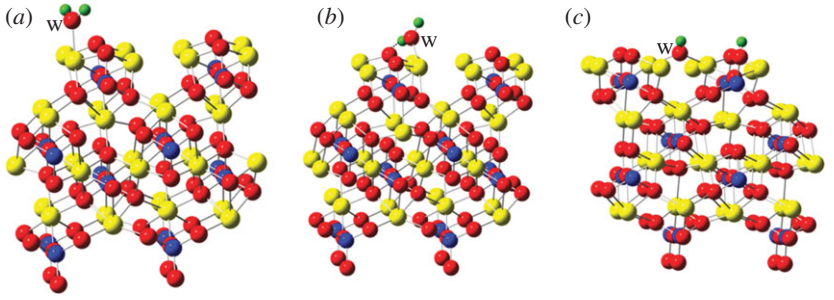

Figure 2. The three most stable adsorption configurations of water on the (100) surface. (*a*) Single site, (*b*) dual site and (*c*) dissociative. Green spheres represent H, and the rest of the representation is as shown in figure 1. The 'w' close to the red sphere indicates O_w.

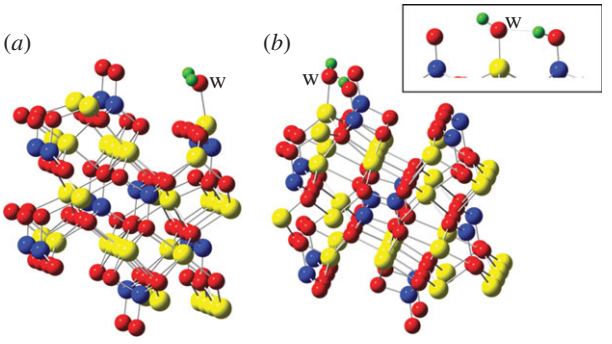

Figure 3. (*a*) The single-site and (*b*) dissociative adsorption of water on the (010) surface. The bonding area is highlighted in the inset. The presentation is as shown in figure 2.

Table 3. Adsorption energy, ΔE (eV) of water on the (100), (001), (010) and (110) surfaces.

		adsorption energy			
adsorption mode	adsorption site/configuration	(100)	(001)	(010)	(110)
associative	Mg/single site	0.76	1.33	0.95	0.95
	Mg/dual site	1.01	1.91	—	—
dissociative	Mg	2.80	1.76	2.05	1.90
	O	—	—	1.64	—

bond with a surface oxygen atom (O_s). The dual-site adsorption is energetically more favourable, owing to an additional hydrogen bond. Further, the Mg−O_w bond lengths are similar to bulk values (table 2), indicating the strong chemical bonding that characterizes associative adsorption. In addition, we also calculated the associative adsorption energetics of the water molecule, when solely mediated by a surface O_s atom. Here, the water molecule either interacted with O_s via O_w or H_w. For both cases, the adsorption energetics was much weaker than the single- or dual-site configurations, and hence is excluded from further consideration.

Dissociation on the (100) surface was observed to be more favourable than associative adsorption; as seen from figure 2, this can be attributed to the fact that the OH binds with two neighbouring Mg atoms on the (100) surface. Other distinct characteristics of dissociation included the fact that the corresponding Mg−O_w bond lengths were much smaller than the

single- or dual-site geometries (table 2), further confirming the much stronger interaction between Mg and OH. Another notable feature was that, energetically, dissociation was found to be independent of the relative positions of the surface Mg and O_s atoms.

(b) Water adsorption on the (001) surface

Similar to the (100) surface, both single- and dual-site adsorption were observed on the (001) surface. The number of active Mg and O_s sites present on the 2×2 supercell surface equalled four each; O_s active sites were either two- or threefold coordinated, with the twofold coordinated O_s being more active owing to their relative under-coordination. The $Mg-O_w$ distance was shorter than the corresponding $Mg-O_w$ bond on the (100) surface and, when viewed in conjunction with the much larger dual-site adsorption energy for (001), it clearly demonstrates that the (001) surface is much more conducive for associative adsorption. Dissociation on the (001) surface is similar to the (100) surface, with the O_w bonding to two surface Mg atoms. Unlike the (100) surface, where all surface Mg atoms were in equivalent sites, the (001) system is characterized by under-coordinated Mg atoms that vary in their distance from the surface. Thus, during dissociation, the O_w creates a strained geometry around the lower Mg atom, leading to a relatively weaker dissociation energy.

(c) Water adsorption on the (010) surface

The (010) surface displayed distinct adsorption characteristics owing to the presence of two onefold coordinated O_s atoms in addition to eight surface Mg atoms (figure 3) for the 2×2 supercell. In particular, the associative adsorption behaviour on the Mg sites was intimately linked to their relative position with respect to the onefolded O_s atoms. Only single-site adsorption was observed, which occurred at surface Mg atoms away from the O_s; by contrast, for the Mg atoms near the onefold coordinated O_s, spontaneous dissociation of the adsorbed water molecule was observed. It has to be noted that the Mg-mediated dissociation adsorption energy for (010) was lower (in magnitude) than that for (100), a direct consequence of the inability of the surface to completely relax owing to the interactions between O_s and O_w; this also results in a larger H_w-O_s bond distance.

A secondary dissociative mechanism was also observed for the (010) surface, exclusively mediated by O_s atoms. The OH interacts with an O_s atom via the O_w, whereas the H_w bonds with another O_s, in addition to a secondary hydrogen bond with the other O_s. The O_w-O_s bond distance in this dissociative adsorption configuration is 1.49 Å.

(d) Water adsorption on the (110) surface

On the (110) surface, single-site associative adsorption was observed, whereas dual-site adsorption was energetically unfavourable. The energy of Mg-mediated dissociation was comparable to that for (001) and (010), with the corresponding $Mg-O_w$ bond distance being much larger than for the other surfaces.

(e) Multi-molecular adsorption

The examination of single water molecule adsorption on forsterite grains clearly demonstrates the efficacy of adsorption as a water-delivery mechanism, based on the high adsorption energies obtained. As a next step, we examined multi-molecular adsorption on the (100) surface, because this system demonstrated the largest adsorption energy among all surfaces. To characterize multi-molecular adsorption, the binding energies were initially calculated for monolayer adsorption, which included up to four water molecules given that the number of O_s equalled four for the 2×2 supercell. For both associative and dissociative monolayer adsorption, a small but systematic decrease (less than 0.04 eV molecule^{-1}) in the respective adsorption energies was observed.

The adsorbed monolayer (dissociated and associated, respectively) was then probed by a water molecule. Irrespective of whether the monolayer was formed via dissociation or association, the second-layer water molecule adsorbed on the underlying monolayer only via physisorption. In particular, the adsorption energy for a second-layer water molecule on the associated and dissociated monolayer was 0.46 and 0.35 eV, respectively, much smaller (in magnitude) than the monolayer adsorption energies. Interestingly, these results are consistent with recent experiments that examined water adsorption on the (100) surface of oriented olivine [23]. In this study, it was shown that the monolayer formed was primarily due to dissociative adsorption, and was very stable even at high temperatures. Further, multi-layer adsorption was very weak and readily desorbed even at a temperature as low as 140 K.

4. Conclusion

The adsorption energetics and geometries of water on (100), (001), (010) and (110) surfaces of forsterite were determined using rigorous DFT-based calculations. Both associative and dissociative adsorptions were individually studied, and the resultant adsorption energies correlated to strong binding. Dissociation was the preferred mode of adsorption for the (100), (010) and (110) surfaces. This work represents an important first step in accurately characterizing the chemical interactions between water-gas and forsterite grains and is central to the construction of larger temporal and spatial-scale models for the quantification of adsorption as a possible delivery mechanism of planetary water.

This work was supported by NASA (grants nos. NNX11AK50G and NNX10AH09G).

References

1. Ciesla F, Lauretta D. 2005 Radial migration and dehydration of phyllosilicates in the solar nebula. *Earth Planet. Sci. Lett.* **231**, 1–8. (doi:10.1016/j.epsl.2004.12.022)
2. Lunine JI, Chambers J, Morbidelli A, Leshin LA. 2003 The origin of water on Mars. *Icarus* **165**, 1–8. (doi:10.1016/S0019-1035(03)00172-6)
3. Morbidelli A, Chambers J, Lunine JI, Petit JK, Robert F, Valsecchi GB, Cyr KE. 2000 Source regions and timescales for the delivery of water to the Earth. *Meteorit. Planet. Sci.* **35**, 1309–1320. (doi:10.1111/j.1945-5100.2000.tb01518.x)
4. Hartogh P *et al.* 2011 Ocean-like water in the Jupiter-family comet 103P/Hartley 2. *Nature* **478**, 218–220. (doi:10.1038/nature10519)
5. Drake MJ. 2005 The Leonard Medal Address: origin of water in the terrestrial planets. *Meteorit. Planet. Sci.* **40**, 519–527. (doi:10.1111/j.1945-5100.2005.tb00960.x)
6. van Boekel R *et al.* 2004 The building blocks of planets within the 'terrestrial' region of protoplanetary disks. *Nature* **428**, 479–482. (doi:10.1038/nature03088)
7. Fegley Jr B. 2000 Kinetics of gas–grain reactions in the solar nebula. *Space Sci. Rev.* **92**, 177–200. (doi:10.1023/A:1005286910756)
8. de Leeuw NH, Catlow CRA, King HE, Putnis A, Muralidharan K, Deymier P, Stimpfl M, Drake MJ. 2010 Where on Earth has our water come from? *Chem. Commun.* **46**, 8923–8925. (doi:10.1039/c0cc02312d)
9. King HE, Stimpfl M, Deymier P, Drake MJ, Catlow CRA, Putnis A, de Leeuw NH. 2010 Computer simulations of water interactions with low-coordinated forsterite surface sites: implications for the origin of water in the inner solar system. *Earth Planet. Sci. Lett.* **300**, 11–18. (doi:10.1016/j.epsl.2010.10.019)
10. Stimpfl M, Walker AM, Drake MJ, de Leeuw NH, Deymier P. 2006 An ångström-sized window on the origin of water in the inner solar system: atomistic simulation of adsorption of water on olivine. *J. Cryst. Growth* **294**, 83–95. (doi:10.1016/j.jcrysgro.2006.05.057)
11. Goumans TPM, Catlow CRA, Brown WA, Kästner J, Sherwood P. 2009 An embedded cluster study of the formation of water on interstellar dust grains. *Phys. Chem. Chem. Phys.* **11**, 5431–5436. (doi:10.1039/b816905e)
12. Muralidharan K, Deymier P, Stimpfl M, de Leeuw NH, Drake MJ. 2008 Origin of water in the inner Solar System: a kinetic Monte Carlo study of water adsorption on forsterite. *Icarus* **198**, 400–407. (doi:10.1016/j.icarus.2008.07.017)

13. Elkins-Tanton LT. 2011 Formation of early water oceans on rocky planets. *Astrophys. Space Sci.* **332**, 359–364. (doi:10.1007/s10509-010-0535-3)
14. Kresse G, Furthmüller J. 1996 Efficiency of *ab initio* total energy calculation for metals and semiconductors using plane-wave basis set. *Comput. Mater. Sci.* **6**, 15–50. (doi:10.1016/0927-0256(96)00008-0)
15. Kresse G, Joubert D. 1999 From ultrasoft pseudopotentials to the projector augmented-wave method. *Phys. Rev. B* **59**, 1758–1775. (doi:10.1103/PhysRevB.59.1758)
16. Perdew JP, Burke K, Ernzerhof M. 1996 Generalized gradient approximation made simple. *Phys. Rev. Lett.* **77**, 3865–3868. (doi:10.1103/PhysRevLett.77.3865)
17. Blöchl PE. 1994 Projector augmented-wave method. *Phys. Rev. B* **50**, 17 953–17 979. (doi:10.1103/PhysRevB.50.17953)
18. Kresse G, Hafner J. 1994 Norm-conserving and ultrasoft pseudopotentials for first-row and transition elements. *J. Phys. Condens. Matter* **6**, 8245. (doi:10.1088/0953-8984/6/40/015)
19. Monkhorst HJ, Pack JD. 1976 Special points for Brillouin-zone integrations. *Phys. Rev. B* **13**, 5188–5192. (doi:10.1103/PhysRevB.13.5188)
20. Fujino K, Sasaki S, Takeuchi Y, Sadanaga R. 1981 X-ray determination of electron distribution in forsterite, fayalite and tephroite. *Acta Crystallogr.* **B37**, 513–518. (doi:10.1107/S0567740881003506)
21. Parker SC, Oliver PM, de Leeuw NH, Titiloye JO, Watson GW. 1997 Atomistic simulation of mineral surfaces: studies of surface stability and growth. *Phase Transit.* **61**, 83–107. (doi:10.1080/01411599708223731)
22. Watson GW, Oliver PM, Parker SC. 1997 Computer simulation of the structure and stability of forsterite surfaces. *Phys. Chem. Miner.* **25**, 70–78. (doi:10.1007/s002690050088)
23. Vattuone L, Smerieri M, Savio L, Asaduzzaman AM, Muralidharan K, Drake MJ, Rocca M. 2013 Accretion disk origin of the Earth's water. *Phil. Trans. R. Soc. A* **371**, 20110585. (doi:10.1098/rsta.2011.0585)